


Cite this: *Catal. Sci. Technol.*, 2017,  
7, 4520

# Direct synthesis of hierarchical ZSM-5 zeolite using cetyltrimethylammonium as structure directing agent for methanol-to-hydrocarbons conversion

Lingqian Meng,<sup>a</sup> Brahim Mezari,<sup>a</sup> Maarten G. Goesten,<sup>†a</sup>  
Wannaruedee Wannapakdee,<sup>ab</sup> Robert Pestman,<sup>a</sup> Lu Gao,<sup>a</sup>  
Jan Wiesfeld<sup>a</sup> and Emiel J. M. Hensen  <sup>\*a</sup>

Hierarchical ZSM-5 zeolite can be obtained in a one-step synthesis approach using cetyltrimethyl-ammonium (CTA) as the sole organic template. The reduced crystal domain size and the presence of mesopores result in improved catalytic performance in methanol-to-hydrocarbon (MTH) reaction as compared to bulk ZSM-5. We investigated the role of the base (LiOH, NaOH, KOH, RbOH, CsOH), the H<sub>2</sub>O/CTA ratio, the Si/Al ratio and counter-ion of CTA (OH<sup>-</sup> vs. Br<sup>-</sup>). The crucial role of KOH and RbOH is evident as only these bases allow dissolution of the amorphous silica-alumina precursor to such extent that zeolite crystallization occurs. With other bases, silica dissolution is too limited to start zeolite crystallization, corroborated by the observation that seeding the synthesis gel rapidly led to mesoporous ZSM-5 zeolite for all bases. With KOH, mesoporous zeolite was obtained in the H<sub>2</sub>O/CTAOH 800–3200 range. The role of Al is also important as without it only ZSM-48 zeolite could be formed, while a too high Si/Al ratio of 20 did not lead to nucleation. A highly crystalline, hierarchical ZSM-5 free from extraframework Al synthesized from a gel with KOH as base, H<sub>2</sub>O/CTAOH and Si/Al ratios of 800 and 50, respectively displayed the highest catalytic performance in the MTH reaction, outperforming bulk ZSM-5.

Received 6th August 2017,  
Accepted 31st August 2017

DOI: 10.1039/c7cy01603d

rsc.li/catalysis

## 1. Introduction

Zeolites are crystalline microporous aluminosilicates commonly used as catalysts, adsorbents and membranes in the chemical industry. They are typically obtained by slow crystallization of silica-alumina gels in which inorganic and/or organic templates direct the structure of the zeolite.<sup>1–10</sup> The void-filling organic templates are called structure-directing agents (SDAs). ZSM-5 is one of the most widely used zeolites and belongs to the pentasil family of zeolites. It contains a three-dimensional 10-membered ring pore system composed of channels and intersections.<sup>11</sup> Notwithstanding the advantages of the microporous nature of zeolites in terms of shape selectivity, the small pore size for ZSM-5 (~5.5 Å) as compared with typical crystal size (0.1–10 μm) usually limits the catalytic

performance due to severe mass transport limitations, as not the entire internal micropore space is effectively used and secondary reactions such as coking can prematurely deactivate the zeolite catalyst by pore blocking.<sup>6,12</sup> Optimizing catalytic performance through tailoring the pore texture of zeolites is currently a very important research topic in academia and industry.<sup>8,13</sup>

Increased mass transport from active sites in the zeolite micropore space to the external surface can for instance be achieved by decreasing the diffusion length, *e.g.*, by shaping zeolite crystals into rods, sheets or nanocrystals. But in ordinary syntheses, such crystals of high aspect ratio are thermodynamically unfeasible due to Ostwald ripening, which is driven by surface tension.<sup>1</sup> The synthesis of hierarchical zeolites in the absence of organic templates has also been achieved recently.<sup>14–16</sup> An alternative approach is to use surfactants that form a liquid crystals at early synthesis times. This topic has been well investigated in the last two decades.<sup>17–22</sup> Surfactants usually have a hydrophilic head group which can serve as a structure-directing moiety in zeolite synthesis, while the hydrophobic tail can be involved in stabilizing textures at the mesoscale. So, cetyltrimethyl-ammonium (CTA, usually charge-stabilized by Br<sup>-</sup> or OH<sup>-</sup>) is up

<sup>a</sup> *Inorganic Materials Chemistry, Schuit Institute of Catalysis, Department of Chemical Engineering and Chemistry, Eindhoven University of Technology, P.O. Box 513, Eindhoven, 5600 MB, The Netherlands. E-mail: e.j.m.hensen@tue.nl*

<sup>b</sup> *Department of Chemical and Biomolecular Engineering, School of Energy Science and Engineering, Vidyasirimedhi Institution of Science and Technology, Rayong 21210, Thailand*

<sup>†</sup> *Current address: Department of Chemistry and Chemical Biology, Cornell University, Baker Lab, 259 East Ave, Ithaca, NY 14850, USA.*



for consideration, as it is an inexpensive, long-tail surfactant, and an analogue of tetramethyl ammonium (TMA), a known SDA in zeolite synthesis.<sup>23</sup>

When CTA's surfactant-like properties were successfully exploited in silica condensation, hexagonal arrays, similar to those in beeswax, of silicate were formed: MCM-41.<sup>24</sup> Yet, the structure does not contain long-range atomic order and the walls are made up of amorphous silica: structure-direction at the meso-scale comes at the cost of microcrystallinity and hydrothermal stability. Afterwards, it was also realized that inclusion of aluminium in these ordered mesoporous silicas did not induce acidity inherent to zeolites and, accordingly, materials like those in the M41S and SBA-n mesoporous silicas are regarded as unfit to replace zeolites in industrial applications.<sup>25–30</sup>

There have been many attempts at synthesizing hierarchical zeolites with CTA. A notable strategy relied on combining a conventional SDA such as tetrapropylammonium for ZSM-5 synthesis with CTA. But the resulting materials are invariably physical mixtures of MCM-41 and zeolite, which shows that two types of SDA do not generally work in concert to generate a hierarchical structure.<sup>25,26</sup> Recently, it has been reported that hierarchical ZSM-5 zeolite can be synthesized in the presence of CTA, albeit it that seeds are required likely to act as a crystal surface on which further zeolite growth occurs.<sup>31–35</sup>

Yet, it remains unclear what obstructs obtaining mesoporous ZSM-5 with CTA directly.<sup>36</sup> Following the breakthrough finding that using the diquatery ammonium surfactant (DQAS) SDAs developed by Ryoo's group can lead to the formation of ZSM-5 zeolite nanosheet.<sup>17</sup> Zhu *et al.* recently showed that the difference between Ryoo's DQAS SDA and CTA resides in fact that the CTA's quaternary ammonium head group fails to enter the inorganic matrix from the very onset of silica condensation, while the diquatery ammonium head group in DAQS SDA shows enforced interaction with the silica matrix already during room temperature mixing of the zeolite synthesis ingredients.<sup>37</sup> Recently, we have demonstrated that replacement of NaOH by KOH facilitates dissolution of silicate from the initially amorphous condensed silica precursor, allowing to obtain highly crystalline hierarchical ZSM-5 zeolites in a single-step synthesis procedure with CTA as the only organic SDA.<sup>38</sup> This approach emphasizes that CTA can act both as an SDA and as a mesoporegen towards hierarchical ZSM-5 formation. The faster crystallization is due to the higher dissolution rate of the mesoporous silica precursor in the presence of KOH. The increased concentration of silicate anions at elevated temperatures induces zeolite nucleation. Thus, hierarchical ZSM-5 zeolite is obtained according to a dissolution–crystallization mechanism rather than a solid–solid transformation. The obtained zeolite showed much higher catalytic performance in the methanol-to-hydrocarbon (MTH) reaction compared with a bulk ZSM-5 sample.

Herein, we investigated the crystallization of gels containing CTA as a SDA and mesoporegen in more detail in order to establish under which conditions direct synthesis of mesoporous ZSM-5 zeolite is possible. We varied the type of base (LiOH, NaOH, KOH, RbOH and CsOH), the CTA concen-

tration, the counter ion of CTA and the Al content. The obtained materials were characterized by elemental analysis, powder X-ray diffraction (XRD), Ar porosimetry, high-resolution scanning electron microscopy (SEM), transmission electron microscopy (TEM) and Fourier transform infrared spectroscopy (FTIR). The catalytic performance of the hierarchical ZSM-5 zeolites was compared with a bulk ZSM-5 zeolite in the MTH reaction.

## 2. Experimental

### 2.1 Sample preparation

Cetyltrimethyl-ammonium hydroxide (CTAOH, TCI, 10 wt%) and cetyltrimethyl-ammonium bromide (CTABr, Aldrich, 95%) were used as received. Ludox AS-40 (Aldrich, 40 wt%) was the silica source in all syntheses. Aluminum hydroxide and all the mineralizing agents (*e.g.* NaOH, KOH) in the work were purchased from Aldrich. Hydrothermal synthesis was performed using the gel compositions given in Table 1. In a standard synthesis, 0.299 g KOH and 3.350 g CTAOH solution were added to 11.085 g demi-water at room temperature. Afterwards, 0.033 g aluminium hydroxide and 3.167 g Ludox AS-40 were added to the mixture under vigorous stirring. The final gel had a molar composition of 5CTA : 12K<sub>2</sub>O : 0.95Al<sub>2</sub>O<sub>3</sub> : 95SiO<sub>2</sub> : 4000H<sub>2</sub>O. After stirring at room temperature for 2 h, the resulting gel was transferred into a 45 mL Teflon-lined steel autoclave and heated under rotating (50 rpm) at 413 K for 6 days. After crystallization, the white product was filtered, washed with demi-water followed by drying overnight at 383 K. The zeolite was calcined at 823 K for 10 h under flowing air to remove the surfactant. The calcined zeolite was ion-exchanged three times with 1.0 M NH<sub>4</sub>NO<sub>3</sub> solutions followed by calcination at 823 K for 4 h in flowing air to obtain the final proton form. For comparison, bulk-ZSM-5 zeolite was synthesized using tetrapropylammonium hydroxide (TPAOH, Merck, 40 wt%) as template.

### 2.2 Characterization

**Elemental analysis.** The elemental composition of the zeolites was determined by ICP-OES (Spectro CirosCCD ICP optical emission spectrometer). For analysis, an equivolumetric mixture of HF (40 wt% in water), HNO<sub>3</sub> (65 wt% in water) and water was used to completely dissolve the zeolites.

**XRD patterns.** XRD patterns were recorded on a Bruker D4 Endeavor using Cu K $\alpha$  radiation with a scanning speed of 0.02° s<sup>-1</sup> in the 2 $\theta$  range of 5–40° and 0.004° s<sup>-1</sup> in the 2 $\theta$  range of 0.7–5°.

**Ar physisorption.** Surface area and porosity of zeolites (H form) were determined by Ar physisorption in static mode at 87 K on a Micromeritics ASAP 2020 instrument. The zeolites were outgassed at 723 K for 6 h prior to the sorption measurements. The BET surface area of ZSM-5 zeolite was determined in the relative pressure range 0.05–0.25. The total pore volume was calculated at  $p/p_0 = 0.97$ . The micropore, mesopore volume and pore size distribution (PSD) of zeolites were determined by the NLDFT method (Ar at 87 K assuming slit pores without regularization).



**Table 1** Summary of synthesis conditions and results

Entry	Molar gel composition				H <sub>2</sub> O	Seed <sup>d</sup>	<i>T</i> (K)	Time (Days)	Morphology
	X <sub>2</sub> O <sup>a</sup>	SiO <sub>2</sub> <sup>b</sup>	Al <sub>2</sub> O <sub>3</sub>	SDA <sup>c</sup>					
MFI(5CTA, K, 0.95Al)	12	95	0.95	5	4000	0	413	6	Meso-ZSM-5
MFI(0CTA, K, 0.95Al)	12	95	0.95	0	4000	0	413	6	Amorphous <sup>e</sup> & α-quartz
MFI(1.25CTA, K, 0.95Al)	12	95	0.95	1.25	4000	0	413	6	Meso-ZSM-5
MFI(2.5CTA, K, 0.95Al)	12	95	0.95	2.5	4000	0	413	6	Meso-ZSM-5
MFI(7.5CTA, K, 0.95Al)	12	95	0.95	7.5	4000	0	413	6	Amorphous
MFI(5CTA, Li, 0.95Al)	12	95	0.95	5	4000	0	413	6	Amorphous & Li <sub>2</sub> Si <sub>2</sub> O <sub>5</sub> <sup>f</sup>
MFI(5CTA, Na, 0.95Al)	12	95	0.95	5	4000	0	413	6	Amorphous
MFI(5CTA, Rb, 0.95Al)	12	95	0.95	5	4000	0	413	6	Meso-ZSM-5
MFI(5CTA, Cs, 0.95Al)	12	95	0.95	5	4000	0	413	6	Amorphous
MFI(5CTA, Li, 0.95Al, seed)	12	95	0.95	5	4000	5	413	6	Meso-ZSM-5 & Li <sub>2</sub> Si <sub>2</sub> O <sub>5</sub>
MFI(5CTA, Na, 0.95Al, seed)	12	95	0.95	5	4000	5	413	6	Meso-ZSM-5
MFI(5CTA, Cs, 0.95Al, seed)	12	95	0.95	5	4000	5	413	6	Meso-ZSM-5
MFI(5CTA, K, 0Al)	12	95	0	5	4000	0	413	6	ZSM-48
MFI(5CTA, K, 0.24Al)	12	95	0.24	5	4000	0	413	6	Meso-ZSM-5
MFI(5CTA, K, 2.38Al)	12	95	2.38	5	4000	0	413	6	Amorphous
MFI(5CTA, K, 2.38Al, seed)	12	95	2.38	5	4000	5	413	6	Meso-ZSM-5
MFI(5CTABr, K, 0.95Al) <sup>g</sup>	12	95	0.95	5	4000	0	413	8	Meso-ZSM-5
bulk-ZSM-5	0	95	0.95	28.5	4275	0	443	5	Bulk-ZSM-5

<sup>a</sup> X = Li, Na, K, Ru or Cs. <sup>b</sup> Tetraethyl orthosilicate as silica source for bulk-ZSM-5 and Ludox AS-40 for the other samples. <sup>c</sup> CTABr for MFI(5CTABr, K, 0.95Al), TPAOH for bulk-ZSM-5, and CTAOH for the other samples. <sup>d</sup> Bulk HZSM-5 as seed. <sup>e</sup> Amorphous silica. <sup>f</sup> Lithium metasilicate. <sup>g</sup> Success rate: 2 out of 5 synthesis.

**Electron microscopy.** Scanning electron microscopy (SEM) images were taken on a FEI Quanta 200F scanning electron microscope at an accelerating voltage of 5 kV. Transmission electron microscopy (TEM) pictures were taken on a FEI Tecnai 20 at 200 kV. The samples were suspended in ethanol and dispersed over a holey Cu grid coated with carbon film prior to measurements.

**FTIR spectroscopy.** FTIR spectra were recorded in the range of 4000–800 cm<sup>-1</sup> by a Bruker Vertex V70v instrument. The spectra were acquired at a 2 cm<sup>-1</sup> resolution and averaged over 64 scans. Typically, an amount of about 10 mg of zeolite was pressed into thin wafers with a diameter of 13 mm and placed inside a controlled-environment infrared transmission cell. Before measurement, the zeolite wafer was firstly heated to 823 K at a rate of 2 K min<sup>-1</sup> in artificial air. Then, the cell was outgassed at the final temperature until the residual pressure was below 5 × 10<sup>-5</sup> mbar. A background IR spectrum was recorded. For CO adsorption, the sample was cooled to 77 K and CO was introduced into the cell *via* a sample loop connected to a Valco six-port valve. After each dosage, a spectrum was recorded at 77 K.

**NMR spectroscopy.** <sup>27</sup>Al Nuclear Magnetic Resonance (NMR) spectra were measured using a 11.7 Tesla Bruker DMX500 NMR spectrometer operating at 132 MHz. The NMR experiments were performed using a Bruker Triple Channel 2.5 mm MAS probe head spinning at 25 kHz. Saturated Al(NO<sub>3</sub>)<sub>3</sub> solution were used for <sup>27</sup>Al NMR shift calibration.

### 2.3 Catalytic activity measurements

The catalytic activity of ZSM-5 zeolites in the MTH reaction was determined in a quartz tubular fixed-bed reactor with an inner diameter of 4 mm. Typically, the proton form of ZSM-5

zeolite was pressed and sieved into 250–425 μm particles. Prior to the reaction, the sample was calcined in the reactor at 823 K in 20 vol% O<sub>2</sub> in He (30 mL min<sup>-1</sup>) for 4 h. The methanol-to-hydrocarbons reaction was performed at 673 K. Methanol (Merck, 99%) was introduced to the reactor by passing a He flow of 30 mL min<sup>-1</sup> through a thermostated saturator. The weight-hourly space velocity (WHSV) of methanol was kept at 6 h<sup>-1</sup>. The product effluent was analyzed on-line by gas chromatography (an Interscience Compact GC equipped with TCD and FID detectors with RT-Q-Bond and Al<sub>2</sub>O<sub>3</sub>/KCl columns). Catalytic lifetime is defined as the time to reach 50% of methanol conversion. Dimethyl ether (DME) was considered as a reactant.<sup>10</sup>

## 3. Results and discussion

### 3.1 Influence of CTA concentration

We first optimized the synthesis of mesoporous ZSM-5 zeolite in the KOH/SiO<sub>2</sub>/CTA system and varied the H<sub>2</sub>O/CTAOH ratio. Fig. 1 shows that crystalline ZSM-5 zeolite can be obtained after 6 days autoclaving at 413 K with a molar H<sub>2</sub>O/CTAOH ratio in the 800–3200 range. Without CTA, only amorphous silica and a small fraction of α-quartz was obtained. The broad feature in the small-angle region of the XRD patterns, observed for all zeolites, is too diffuse to be correlated to any sort of symmetry although it hints at partial order at the mesoscale. The order increases with rising CTA concentration. At the highest CTA concentration, crystallization did not occur and only amorphous silica was formed.

The SEM images in Fig. 2A show substantial differences in the morphology among the materials. Without CTA in the gel, the obtained material exhibits two morphologies, namely that of nanolayers and nanoparticles, which are assumed to be



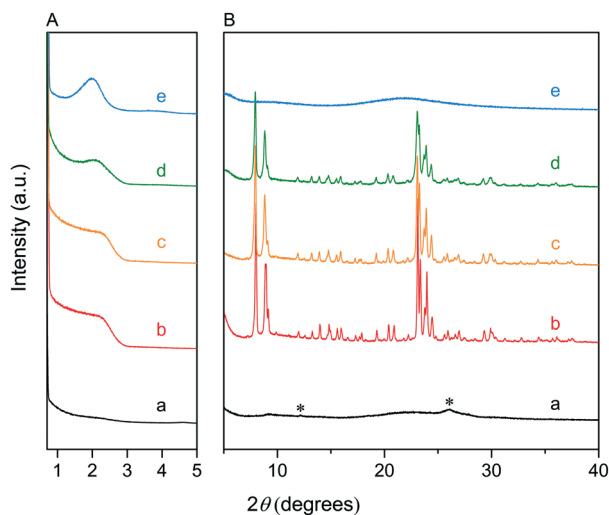


**Fig. 1** (A) Small-angle and (B) wide-angle powder XRD patterns of the as-synthesized samples from a composition gel of  $K_2O : SiO_2 : Al_2O_3 : CTAOH : H_2O = 12 : 95 : 0.95 : x$  ( $x = 0, 1.25, 2.5, 5, 7.5$ ):4000. (a) MFI(0CTA, K, 0.95Al), (b) MFI(1.25CTA, K, 0.95Al), (c) MFI(2.5CTA, K, 0.95Al), (d) MFI(5CTA, K, 0.95Al) and (e) MFI(7.5CTA, K, 0.95Al). \*Characteristic pattern for  $\alpha$ -quartz.

related to  $\alpha$ -quartz<sup>39</sup> and amorphous silica, respectively. The three zeolites have the morphology of agglomerated nanocrystals. Increasing the surfactant CTAOH concentration in the synthesis gel led to a decreased crystal size. This emphasizes the role of CTA as mesoporegen during crystallization. In Ar physisorption (Fig. 2B), the ZSM-5 zeolites MFI(2.5CTA, K, 0.95Al) and MFI(5CTA, K, 0.95Al) display a clear hysteresis loop and a climbing slope at the intermediate pressure range. The loop does not close until the relative pressure is quite close to the saturation pressure. The hysteresis is more pronounced with increasing CTA concentration in the gel. According to IUPAC classifications, the two isotherms are of the IV shape with a H4 hysteresis loop,<sup>40,41</sup> which is generally attributed to a hierarchical porous material containing both micropores and mesopores. The strong uptake at low relative pressure certifies the presence of micropores.<sup>40</sup> Differently, the zeolite MFI(1.25CTA, K, 0.95Al) has a type I isotherm. The limited Ar uptake after the initial uptake in the micropores indicates the low external/mesopore surface area. As common estimations for the pore size distribution (PSD) such as the BJH method are considered unreliable for isotherms containing H4-type hysteresis loops,<sup>40</sup> we employed the NLDFT method assuming slit-shaped pores without regulation. A distinct peak at  $\sim 0.53$  nm in the PSDs of all the zeolites (Fig. 2C) corresponds to the pore size of ZSM-5 zeolites. There is also a wide distribution of larger pores, stretching into the mesopore range up to 40 nm. The corresponding textural properties are listed in Table 2. The total pore volume and the mesopore volume of the zeolites follow the sequence: MFI(1.25CTA, K, 0.95Al) < MFI(2.5CTA, K, 0.95Al) < MFI(5CTA, K, 0.95Al), indicating the importance of CTA for generating mesopores in zeolites. Consistent with the high crystallinity of these three samples, their micropore volume is similar. Both the isotherms and shape of the PSDs fit

our SEM analysis, emphasizing that the secondary set of pores in the zeolites originates from voids between intergrown nanocrystals.

The three HZSM-5 zeolites were evaluated as catalysts for the MTH reactions (Fig. 2D). Details including the product distribution after 1 h time on stream are listed in Table 3. The catalytic performance of bulk-ZSM-5 with similar Al content (Table 2) was included for comparison. Methanol conversion was complete for all the zeolites at the beginning of the reaction. The lifetime of the zeolites in MTH reaction follows the sequence: bulk-ZSM-5 < MFI(1.25CTA, K, 0.95Al) < MFI(2.5CTA, K, 0.95Al) < MFI(5CTA, K, 0.95Al), indicating that the additional porosity strongly enhances the catalyst lifetime. The main products of the three zeolites after 1 h time on stream are ethylene, propylene and  $C_{4+}$  products, as typically observed for methanol conversion by ZSM-5 zeolites.<sup>42–44</sup> Although the exact nature of the “hydrocarbon pool” species in the MTH reaction remains unclear,<sup>45–48</sup> it is widely accepted that ethylene selectivity can be used for assessing the importance of the propagation *via* polymethylated benzenes, while  $C_{4+}$  selectivity is considered as an indicator for the degree of propagation *via* the olefins-based cycle.<sup>10,49</sup> A salient detail noted from the data in Table 3 is that the  $C_{4+}$ /ethylene ratio of the ZSM-5 zeolites increased in the order: MFI(1.25CTA, K, 0.95Al) < MFI(2.5CTA, K, 0.95Al) < MFI(5CTA, K, 0.95Al). Thus, the olefins-based cycle appears to become more important with increasing mesoporosity. We tentatively attribute this to a shorter intracrystalline residence time of aromatics with decreasing crystalline domain size. The increasing mesoporosity is due to a smaller crystalline domain size.

### 3.2 Influence of base

Fig. 3A and B respectively show the small- and wide-angle XRD patterns of the as-synthesized materials using different bases. Similar with the standard synthesis procedure, the XRD pattern of the sample synthesized in the presence of RbOH instead of KOH is characteristic for MFI zeolite. The electron microscopy images (Fig. 3C and D) show that the MFI(5CTA, Rb, 0.95Al) sample is made up from aggregates of MFI nanocrystals. The Ar physisorption isotherm in Fig. 4A is of type IV with a H1 hysteresis loop. According to literature, such hysteresis loop is often associated with porous materials exhibiting a narrow distribution of relatively uniform cylindrical-like pores.<sup>40,41</sup> In accordance with this, the PSD of this material (Fig. 4B) shows a sharp peak centered at about 3.75 nm in the mesopore range. The textural properties collected in Table 2 show that the hierarchical ZSM-5 possesses higher total pore volume and mesopore volume in comparison with the bulk-ZSM-5 zeolite. On the other hand, the micropore volumes of these two zeolites are comparable, justifying the conclusion that the crystallinity of MFI(5CTA, Rb, 0.95Al) is high. Important for our later comparison of the catalytic performance of these samples in the MTH reaction, Table 2 shows that the MFI(5CTA, Rb, 0.95Al) possesses similar framework Al content as the bulk-ZSM-5 sample. Fig. 4C



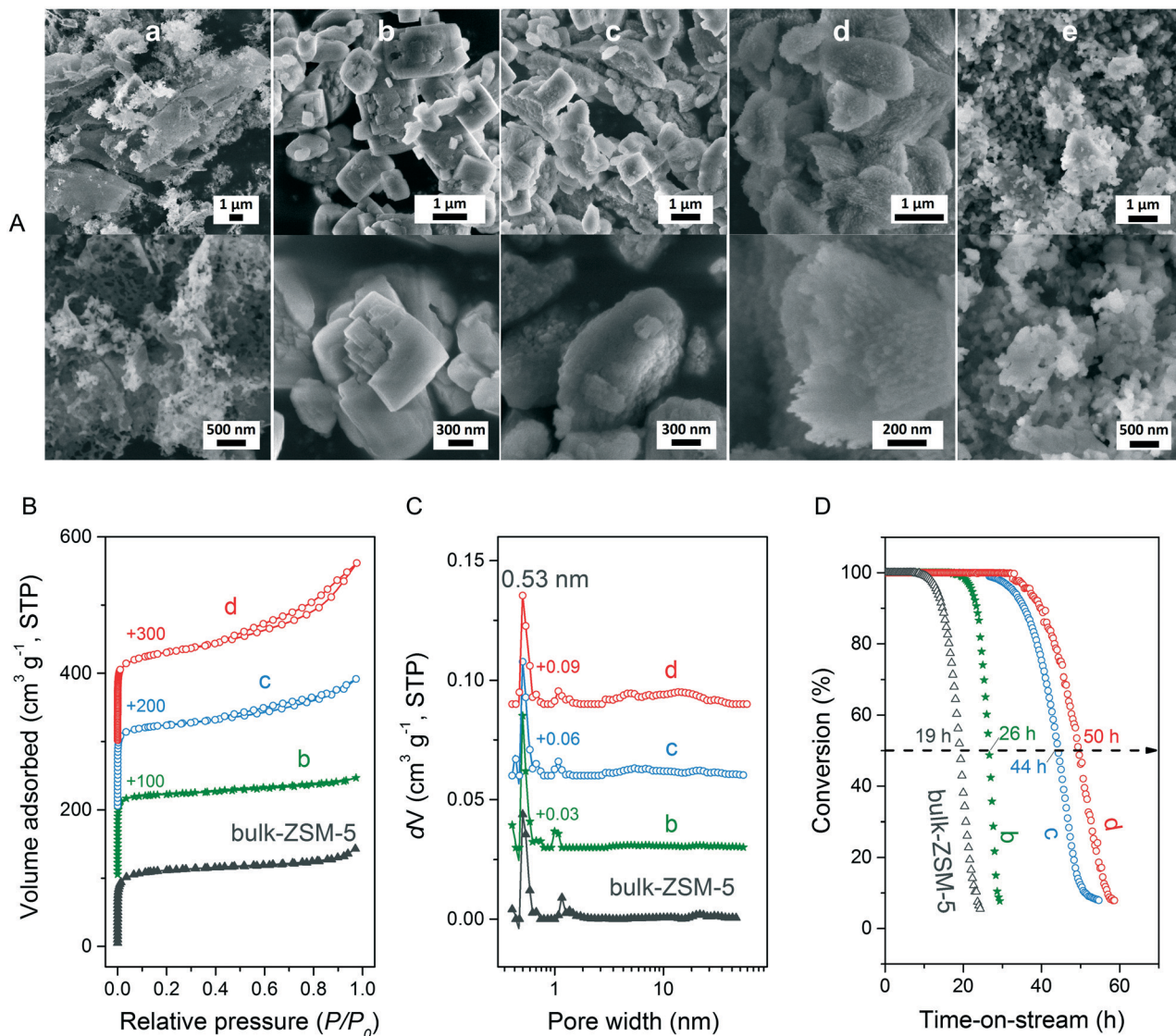


**Fig. 2** (A) SEM images of the as-synthesized samples; (B) Ar physisorption isotherm, (C) the corresponding pore size distribution, and (D) methanol conversion as a function of time on stream for the three zeolites (H form) as well as bulk-ZSM-5 in the MTH reaction. (a) MFI(0CTA, K, 0.95Al), (b) MFI(1.25CTA, K, 0.95Al), (c) MFI(2.5CTA, K, 0.95Al), (d) MFI(5CTA, K, 0.95Al) and (e) MFI(7.5CTA, K, 0.95Al). Catalytic lifetime is defined as the time to reach 50% of methanol conversion. Dimethyl ether (DME) was considered as a reactant.

**Table 2** Textural properties of the zeolites

Sample	Al content <sup>a</sup> (%)	Al <sub>framework</sub> <sup>b</sup> (%)	$S_{\text{BET}}$ <sup>c</sup> ( $\text{m}^2 \text{g}^{-1}$ )	$V_{\text{total}}$ <sup>d</sup> ( $\text{cm}^3 \text{g}^{-1}$ )	$V_{\text{meso}}$ <sup>e</sup> ( $\text{cm}^3 \text{g}^{-1}$ )	$V_{\text{micro, NLDFT}}$ <sup>f</sup> ( $\text{cm}^3 \text{g}^{-1}$ )
MFI(5CTA, K, 0.95Al)	0.94	87	401.5	0.34	0.11	0.12
MFI(1.25CTA, K, 0.95Al)	1.28	78	341.4	0.17	0.02	0.13
MFI(2.5CTA, K, 0.95Al)	1.14	93	347.6	0.22	0.06	0.12
MFI(5CTA, Rb, 0.95Al)	1.10	77	445.3	0.35	0.19	0.11
MFI(5CTA, K, 0Al)	0.00	—	233.5	0.40	0.35	0.02
MFI(5CTA, K, 0.24Al)	0.31	47	468.5	0.32	0.14	0.13
MFI(5CTA, K, 2.38Al, Seed)	2.56	83	414.5	0.37	0.24	0.11
MFI(5CTABr, K, 0.96Al)	0.97	84	476.8	0.26	0.11	0.12
bulk-ZSM-5	1.12	86	347.2	0.18	0.02	0.12

<sup>a</sup> Determined using ICP-OES analysis. <sup>b</sup> Fraction of framework Al determined by <sup>27</sup>Al NMR.<sup>50</sup> <sup>c</sup> Brunauer–Emmett–Teller (BET) surface area ( $p/p_0 = 0.05–0.25$ ). <sup>d</sup> Total pore volume at  $p/p_0 = 0.97$ . <sup>e</sup> Mesopore volume and <sup>f</sup> micropore volume calculated by the NLDFT method using the adsorption branch of the isotherm (Ar at 87 K assuming slit pores without regularization).

illustrates that the MFI(5CTA, Rb, 0.95Al) has a longer lifetime in MTH reaction than the bulk-ZSM-5 zeolite, which is

mainly due to the hierarchical structure of the zeolite in line with earlier findings for mesoporous ZSM-5 synthesized by



**Table 3** Lifetime and product selectivities of ZSM-5 zeolite catalysts for the MTH reaction after 1 h time on stream

Zeolite	Lifetime <sup>a</sup> (h)	Selectivity (%)						Aromatics
		CH <sub>4</sub>	C <sub>2</sub> <sup>=</sup>	C <sub>2</sub>	C <sub>3</sub> <sup>=</sup>	C <sub>3</sub>	C <sub>4+</sub>	
MFI(5CTA, K, 0.96Al)	50	0.3	7.8	0.1	35.3	2.3	49.0	5.2
MFI(1.25CTA, K, 0.96Al)	26	0.6	14.1	0.3	35.9	5.2	41.8	1.0
MFI(2.5CTA, K, 0.96Al)	44	1.0	11.8	0.1	37.4	3.8	43.6	1.6
MFI(5CTA, Rb, 0.96Al)	34	0.3	6.7	0.2	41.9	1.1	46.6	3.3
MFI(5CTA, Li, 0.96Al, seed)	—	0.8	5.1	<0.1	25.4	<0.1	39.7	28.8
MFI(5CTA, Na, 0.96Al, seed)	89	0.5	8.9	<0.1	38.7	2.9	46.8	2.0
MFI(5CTA, Cs, 0.96Al, seed)	—	0.3	5.0	0.3	51.1	1.0	36.0	6.3
MFI(5CTA, K, 0.28Al)	—	1.2	3.6	0.2	52.0	0.3	32.0	9.9
MFI(5CTA, K, 2.38Al, seed)	—	0.6	8.2	0.1	30.0	3.9	44.7	12.5
MFI(5CTABr, K, 0.96Al)	46	0.3	6.8	0.5	37.5	1.6	53.3	2.2
bulk-ZSM-5	19	0.4	9.8	0.1	31.1	3.7	54.8	0.1

<sup>a</sup> Time to reach methanol conversion of 50%, DME was considered as reactant. WHSV = 6 h<sup>-1</sup>; T = 673 K.

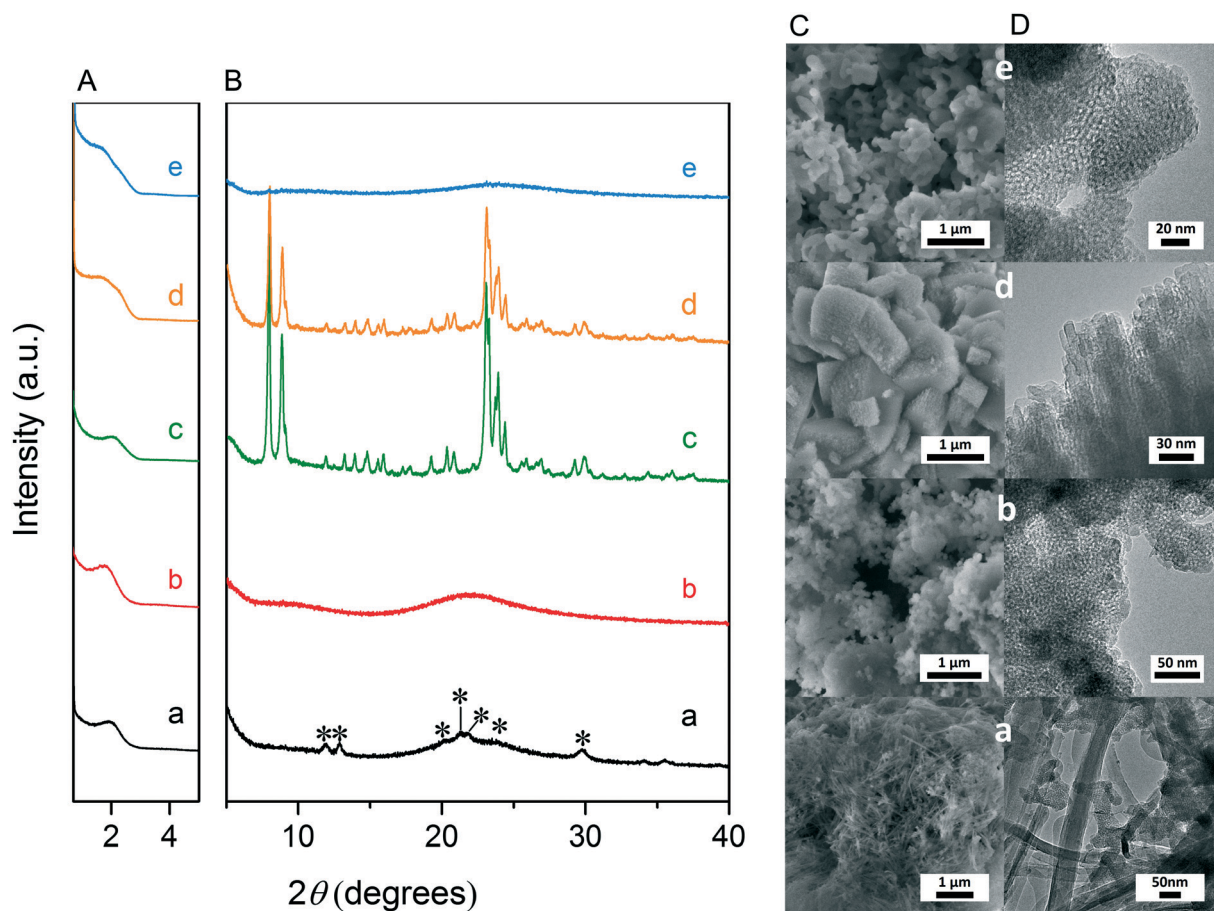


**Fig. 3** (A) Small-angle and (B) wide-angle powder XRD patterns; (C) SEM and (D) TEM images of the as-synthesized materials. (a) MFI(5CTA, Li, 0.95Al), (b) MFI(5CTA, Na, 0.95Al), (c) MFI(5CTA, K, 0.95Al), (d) MFI(5CTA, Rb, 0.95Al) and (e) MFI(5CTA, Cs, 0.95Al). The molar ratio of the composition in the gel is X<sub>2</sub>O (K<sub>2</sub>O, Li<sub>2</sub>O, Na<sub>2</sub>O, Rb<sub>2</sub>O, Cs<sub>2</sub>O):SiO<sub>2</sub>:Al<sub>2</sub>O<sub>3</sub>:CTAOH:H<sub>2</sub>O = 12:95:0.95:5:4000. \*Characteristic pattern for lithium metasilicate (Li<sub>2</sub>Si<sub>2</sub>O<sub>5</sub>).

standard procedure.<sup>10</sup> Importantly, compared with bulk-ZSM-5, the higher C<sub>4+</sub>/ethylene ratio of MFI(5CTA, Rb, 0.95Al) in the product selectivities (Table 3) indicates the higher contribution of the olefins-based cycle in methanol conversion. Interestingly, although with substantial mesoporosity, the MFI(5CTA, Rb, 0.95Al) displays much shorter

lifetime than MFI(5CTA, K, 0.95Al) synthesized in the presence of KOH.

When the same syntheses were carried out with NaOH or CsOH in the gel, the XRD patterns of the obtained materials were that of amorphous silica.<sup>50</sup> The use of LiOH as base resulted in the mixture of amorphous silica and lithium



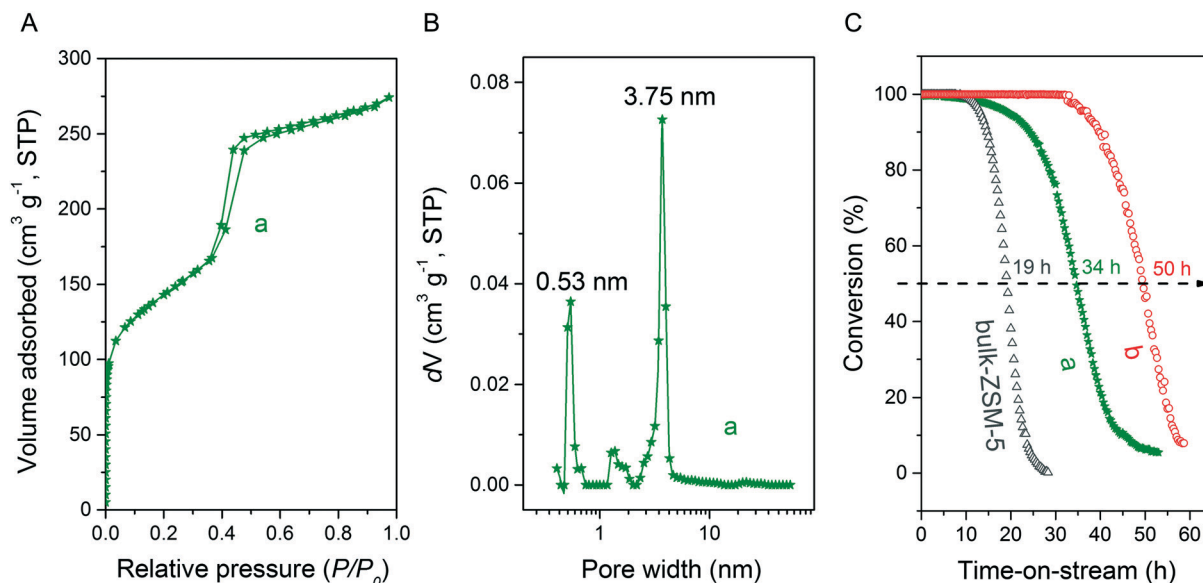


Fig. 4 (A) Ar physisorption isotherm, (B) the corresponding pore size distribution and (C) the methanol conversion as a function of time on stream for the MFI(5CTA, Rb, 0.95Al) zeolite (H form) in the MTH reaction. The zeolite was synthesized from a composition gel of Rb<sub>2</sub>O:SiO<sub>2</sub>:Al<sub>2</sub>O<sub>3</sub>:CTAOH:H<sub>2</sub>O = 12:95:0.95:5:4000. Catalytic performance of bulk-ZSM-5 and MFI(5CTA, K, 0.95Al) in MTH reaction was also shown in Fig. 4C for comparison.

metasilicate.<sup>51</sup> The lithium metasilicate part consists of nano-rods with a thickness around 50 nm.

A tentative mechanism for the growth of these hierarchical zeolites in the presence of different bases is shown in Fig. 5.

Upon ageing the gel at room temperature, an amorphous silica-alumina precursor is formed in which the negatively charged silicate surface is compensated by alkali and CTA cations.<sup>52</sup> It has been demonstrated before that, compared

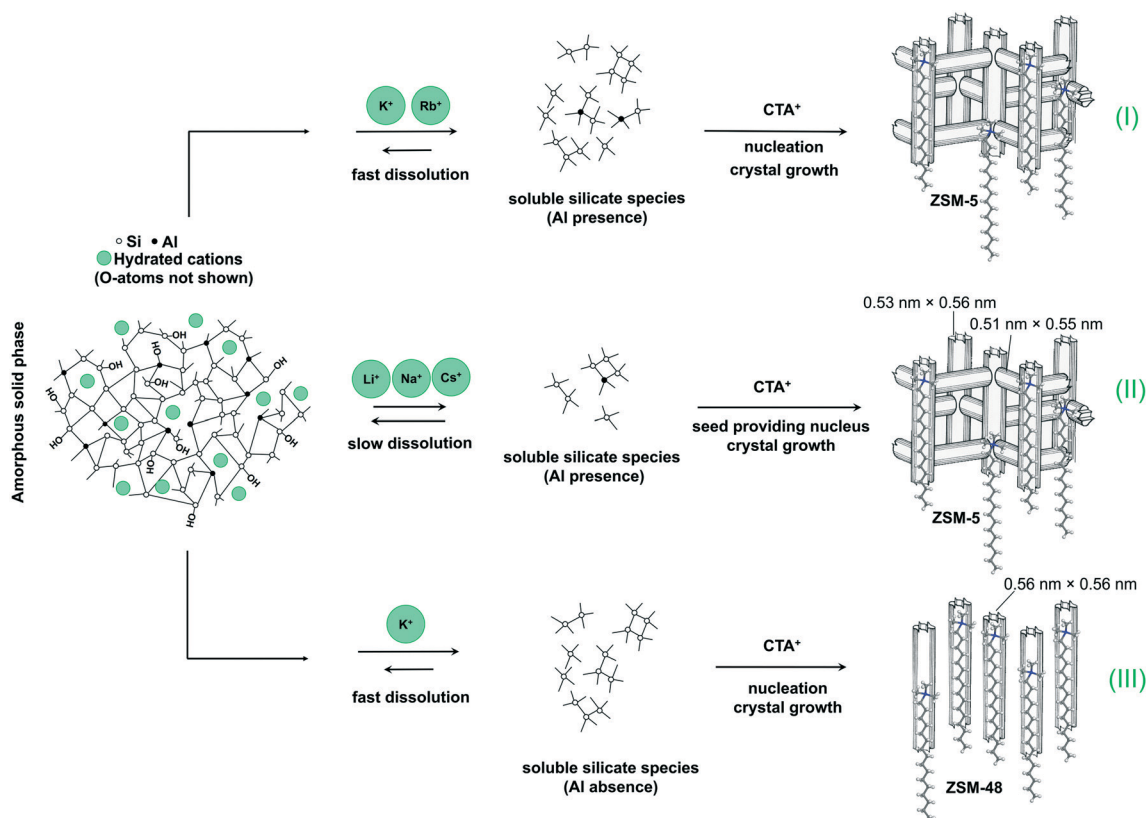


Fig. 5 The mechanism of hierarchical ZSM-5 zeolite and ZSM-48 zeolite formation.



with  $\text{Cs}^+$  and  $\text{Li}^+$ ,  $\text{K}^+$  and  $\text{Rb}^+$  favor dissolution of silicate species from amorphous silica to form monomeric silicate species.<sup>53,54</sup> We argue that (super)saturation of soluble (monomeric and oligomeric) silicate species will therefore occur easier and so does nucleation.<sup>54</sup> As discussed earlier, nucleation likely involves the interaction of silicate species with the quaternary ammonium head group of CTA. The hydrophobic tails then have the effect of interrupting zeolite growth, resulting in final hierarchical ZSM-5 zeolite. Another aspect of the work of Van Santen and co-workers is that TMA also slows silica dissolution. This explains the recalcitrance to crystallization at high CTA concentration in our study.

To further support the hypothesis that nucleation is indirectly inhibited by the stabilization of the silica–alumina precursor by  $\text{Li}^+$ ,  $\text{Na}^+$  and  $\text{Cs}^+$  ions, a small amount of HZSM-5 seeds was added to the synthesis gel (Fig. 5).<sup>55</sup> From the XRD patterns in Fig. 6, we can see that in all the three cases ZSM-5 zeolite was obtained after 6 days of hydrothermal synthesis. Interestingly, the morphologies of these three materials are quite different. MFI(5CTA, Li, 0.96Al, seed) contains ZSM-5 particles and certain impurities of rod-like lithium metasilicate. MFI(5CTA, Na, 0.96Al, seed) is composed of aggregated nanoparticles (<50 nm), while the MFI(5CTA, Cs, 0.96Al, seed) zeolite is not uniform in morphology, containing nanolayers and nanoparticles. Correspondingly, the catalytic performance of these three materials (H form) in MTH reaction differs significantly. MFI(5CTA, Na, 0.96Al, seed) had a lifetime as high as 89 h. Although initial methanol conversion reached 97%, the MFI(5CTA, Cs, 0.96Al, seed) zeolite started to deactivate already after 5 min time on stream. MFI(5CTA, Li, 0.96Al, seed) only converted 42% of

methanol in the initial time on stream, and its catalytic activity decreased dramatically in 24 h reaction.

### 3.3 Influence of Al content

We also varied the Al content in the synthesis gel. XRD shows that without Al in the gel phase-pure ZSM-48 zeolite is obtained. This zeolite has the \*MRE topology comprised of a tubular pore system with pore diameter of  $0.56 \text{ nm} \times 0.56 \text{ nm}$ .<sup>56,57</sup> The corresponding SEM (Fig. 8A and B) and TEM (Fig. 8C) images show that the obtained ZSM-48 zeolite is composed of aggregated nanowires with a thickness of about 20 nm. According to the database of the Structure Commission of the International Zeolite Association (IZA-SC), both MFI and \*MRE frameworks contain the composition building unit of *mel*. Besides, the MFI structure contains *mor* (*t-tes*), *cas* and *mfi* (*t-pen*) units, while the \*MRE topology contains *imf* (*t-imf-7*) and *afi* (*t-afi*) units. These units are shown in Fig. 9. We hypothesize that under our synthesis conditions, in the initial nucleation stage of zeolite formation, the presence of Al is necessary for forming part of/all *mor* (*t-tes*)/*cas*/*mfi* (*t-pen*) units, which results in further MFI zeolite growth. Instead, in the absence of Al the units of *imf* (*t-imf-7*) and *afi* (*t-afi*) are formed for further \*MRE zeolite growth. Fig. 10 displays the Ar physisorption isotherm and corresponding PSD of calcined ZSM-48. A type IV isotherm can be seen with a distinct H1 hysteresis loop at very narrow relative pressure range between  $p/p_0 = 0.35$  and  $0.65$ , which indicates a narrow distribution of mesopores.<sup>40</sup> A weak uptake at low relative pressure is indicative of the low micropore volume. In line with this, there is no clear feature related to micropores in

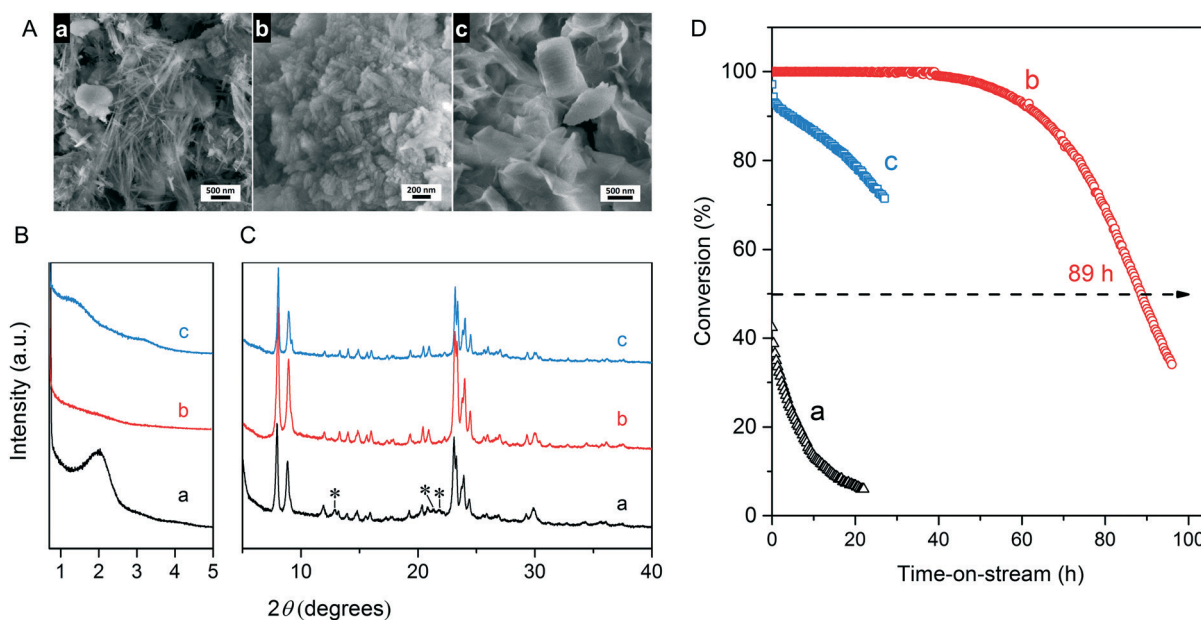


**Fig. 6** (A) SEM images, (B) small-angle and (C) wide-angle powder XRD patterns of as-synthesized materials; (D) methanol conversion over the H form of three zeolites. (a) MFI(5CTA, Li, 0.96Al, seed) (b) MFI(5CTA, Na, 0.96Al, seed) and (c) MFI(5CTA, Cs, 0.96Al, seed). The molar ratio of the composition gel is  $\text{Li}_2\text{O}$  (or  $\text{Na}_2\text{O}$ ,  $\text{Cs}_2\text{O}$ ): $\text{SiO}_2$ : $\text{Al}_2\text{O}_3$ :CTAOH: $\text{H}_2\text{O}$ :seed = 12:95:0.95:5:4000:5. \*Characteristic pattern for lithium metasilicate.





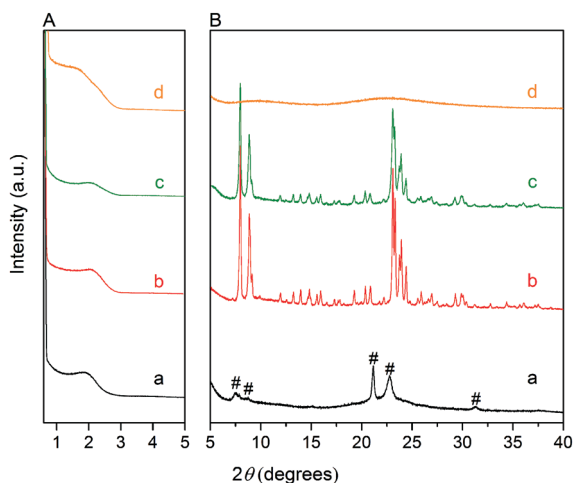


**Fig. 7** (A) Small-angle and (B) wide-angle powder XRD patterns of samples synthesized from a composition gel of  $K_2O:SiO_2:Al_2O_3:CTAOH:H_2O = 12:95:x$  ( $x = 0, 0.24, 0.95, 2.38$ ):5:4000. (a) MFI(5CTA, K, 0Al), (b) MFI(5CTA, K, 0.24Al), (c) MFI(5CTA, K, 0.95Al) and (d) MFI(5CTA, K, 2.38Al). #Characteristic pattern for ZSM-48 zeolite.

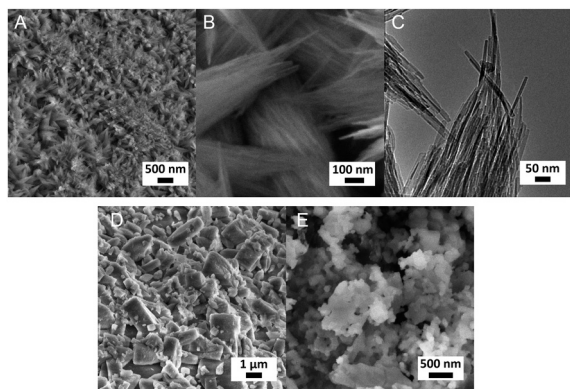


**Fig. 8** (A, B, D and E) SEM images, and (C) TEM image of samples synthesized from a composition gel of  $K_2O:SiO_2:Al_2O_3:CTAOH:H_2O = 12:95:x$  ( $x = 0, 0.24, 2.38$ ):5:4000. (A-C) MFI(5CTA, K, 0Al), (D) MFI(5CTA, K, 0.24Al) and (E) MFI(5CTA, K, 2.38Al).

the PSD. A distinct peak centered around 3.4 nm can be ascribed to the uniform voids between nanorods, which is inconsistent with the display of a hysteresis loop in a narrow relative pressure range. The corresponding textural properties are listed in Table 2. The nano-rod ZSM-48 zeolite has a total pore volume and a mesopore volume of  $0.40 \text{ cm}^3 \text{ g}^{-1}$  and  $0.35 \text{ cm}^3 \text{ g}^{-1}$ , respectively. The BET surface area is about  $234 \text{ m}^2 \text{ g}^{-1}$ . The micropore volume is only  $0.02 \text{ cm}^3 \text{ g}^{-1}$ .

Interestingly, the XRD pattern confirms that the addition of a small amount of Al in the gel ( $Si/Al = 200$ ) already changed the outcome of the synthesis towards formation of ZSM-5 zeolite instead of ZSM-48. The MFI(5CTA, K, 0.24Al) sample only contains 0.31 wt% of Al according to elemental analysis, with about half of it ending up in framework positions after calcination (Table 2). SEM (Fig. 8D) shows that MFI(5CTA, K, 0.24Al) is not uniform in particle size. Ar physisorption presents a clear H4 hysteresis loop in the type-

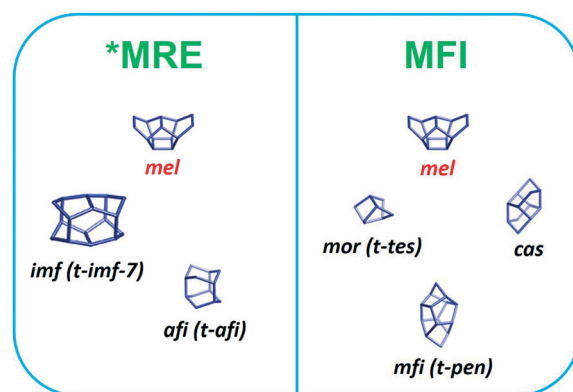


**Fig. 9** Composite building units of \*MRE and MFI zeolites according to database of the Structure Commission of the International Zeolite Association.

IV isotherm with a narrow PSD in the mesopore range centered at about 3.4 nm (Fig. 10A and B). The distinct peak at 0.53 nm is in line with the pore size of MFI topology. A salient detail noted from the data in Table 2 is that MFI(5CTA, K, 0.24Al) zeolite possesses a high mesopore volume of  $0.14 \text{ cm}^3 \text{ g}^{-1}$ . The micropore volume is  $0.13 \text{ cm}^3 \text{ g}^{-1}$ , similar with that of bulk-ZSM-5. Due to the low Al content, the methanol conversion was not complete for this hierarchical ZSM-5 at the start of the MTH reaction, although it presented a good stability (Fig. 10C). This may be due to the lower acid site density which implies a lower rate of secondary reactions leading to coke.<sup>43</sup> Secondly, the hierarchical pore system leads to the enhanced utilization of Brønsted acid sites in the inner crystal particles.<sup>50,58</sup> Similar with the bulk-ZSM-5, the main products were ethylene, propylene and  $C_{4+}$  products after 1 h time on stream. The product distribution was shifted to propylene and aromatics instead of ethylene and higher olefins.

Setting the  $Si/Al$  ratio to 20 in the synthesis gel, the obtained MFI(5CTA, K, 2.38Al) material shows a broad peak between  $15\text{--}35^\circ$  in XRD pattern (Fig. 7), which is typical for amorphous silica.<sup>50</sup> The corresponding SEM image confirms that MFI(5CTA, K, 2.38Al) consists of nanoparticles. A tentative explanation is that the high Al content of the solid precursor binds the cations strongly so that dissolution is slowed down and therefore no supersaturation as well as nucleation is reached. To confirm this hypothesis, a small amount of ZSM-5 seeds was added into the gel. As expected, the obtained material shows the characteristic XRD pattern of MFI zeolite (Fig. 11A). Importantly, the broadening of the reflections between  $22\text{--}25^\circ$  are indicative of the small crystal domain size.<sup>9</sup> In agreement with this, the SEM images (Fig. 11B) show that the zeolites are aggregated nano-needles with a uniform thickness about 20 nm. The proton-form of this zeolite shows a distinct H1 type hysteresis loop in the Ar physisorption isotherm (Fig. 11D), indicating the presence of uniform mesopores. The PSD displays two peaks centered at 0.53 nm and 4.0 nm, which can be related to MFI micropores and uniform voids between the nano-needles, respectively.



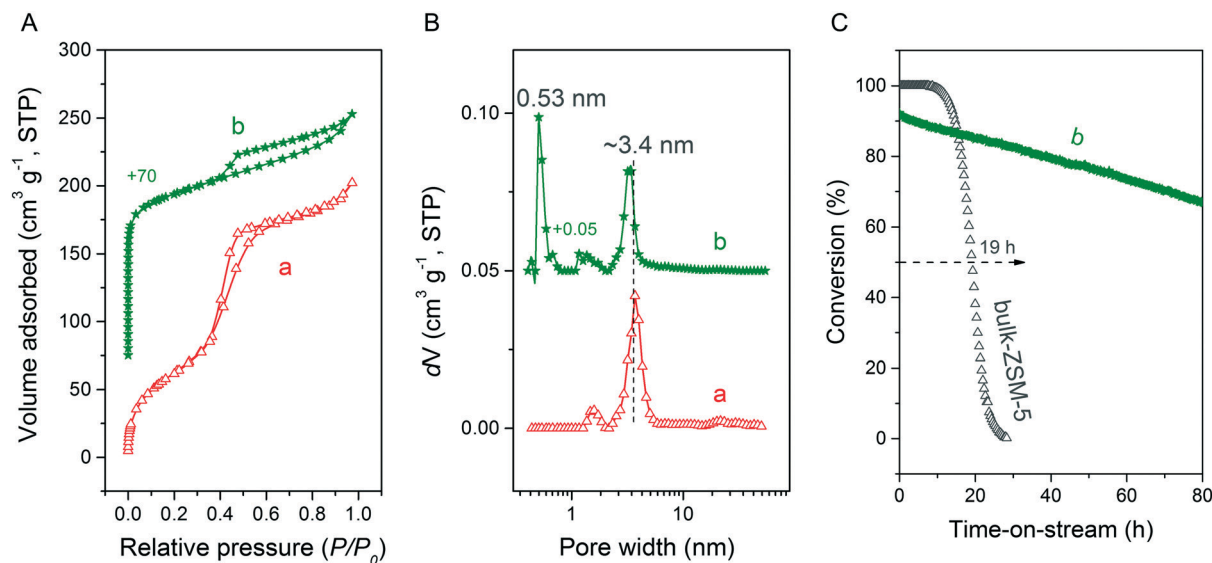


Fig. 10 (A) Ar physisorption isotherm and (B) PSD of calcined (a) MFI(5CTA, K, 0Al) and (b) MFI(5CTA, K, 0.24Al); (C) methanol conversion as a function of time on stream over bulk-ZSM-5 and MFI(5CTA, K, 0.24Al) (H form).

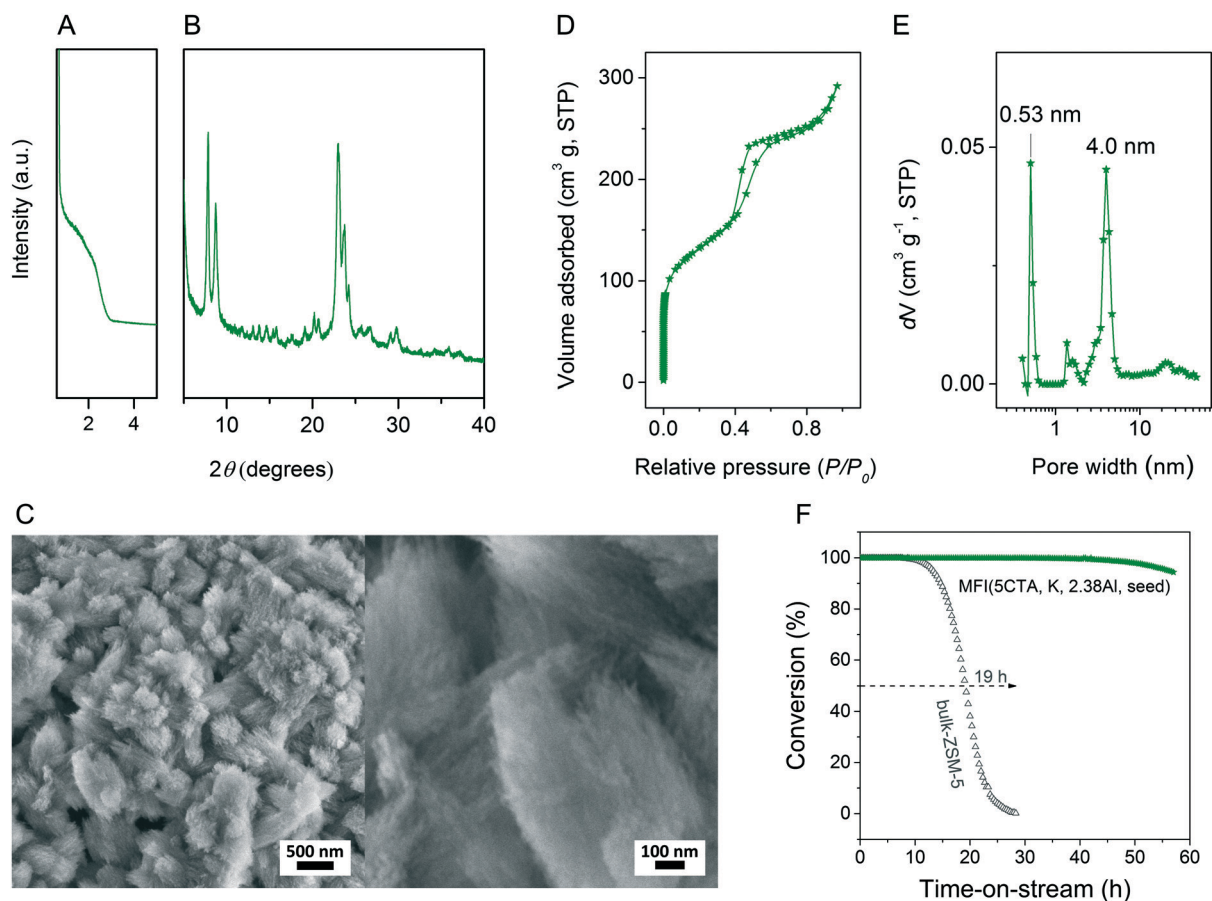


Fig. 11 (A) Small-angle and (B) wide-angle powder XRD patterns and (C) SEM images of as-synthesized MFI(5CTA, K, 2.38Al, seed); (D) Ar physisorption isotherm, (E) PSD and (F) methanol conversion as a function of time on stream over MFI(5CTA, K, 2.38Al, seed) (H form). The zeolite was synthesized from a composition gel of K<sub>2</sub>O : SiO<sub>2</sub> : Al<sub>2</sub>O<sub>3</sub> : CTAOH : H<sub>2</sub>O : seed = 12 : 95 : 2.38 : 5 : 4000 : 5. Methanol conversion over bulk-ZSM-5 was shown in (F) for comparison.

The corresponding textural properties are listed in Table 2. Consistent with its high crystallinity, the micropore volume

of MFI(5CTA, K, 2.38Al, seed) is similar with that of bulk-ZSM-5. In contrast, the hierarchical zeolite contains



significantly higher mesopore volume ( $0.24 \text{ cm}^3 \text{ g}^{-1}$ ) and total pore volume ( $0.37 \text{ cm}^3 \text{ g}^{-1}$ ) than its bulk counterpart. According to  $^{27}\text{Al}$  NMR spectroscopy, most of the Al ends up in the zeolite framework position for such high Al content. Compared with bulk-ZSM-5, MFI(5CTA, K, 2.38Al, seed) shows pronounced stability in the MTH reaction. The deactivation only occurs after 40 h time on stream. Especially, the aromatics selectivity is much higher than for bulk-ZSM-5. This is ascribed to the higher reaction rates of oligomerization, cyclization and dehydrogenation of olefins in zeolite channels that contain more Brønsted acid sites.<sup>44</sup>

### 3.4 Influence of CTA counter-ion

We also verified the outcome of the synthesis when CTAOH was replaced by CTABr. The wide-angle XRD patterns (Fig. 12B) confirm that pure MFI zeolite was obtained after 8 days hydrothermal synthesis using CTABr as SDA. Compared with the standard recipe in which highly crystallized MFI zeolite was obtained after 6 days hydrothermal synthesis using CTAOH as the SDA, the application of CTABr as SDA slows the crystallization slightly and about 8 days are required to obtain highly crystalline zeolite. The broad peak in the small-angle XRD patterns (Fig. 12A) evidence the partially ordered mesoporosity of MFI(CTABr, K, 0.96Al). SEM (Fig. 12C) and TEM (Fig. 12D) images show that the zeolite consists of agglomerated nano-particles with dimensions in the range of 20–50 nm. These images also show mesoporous voids between the primary particles. We mention that in

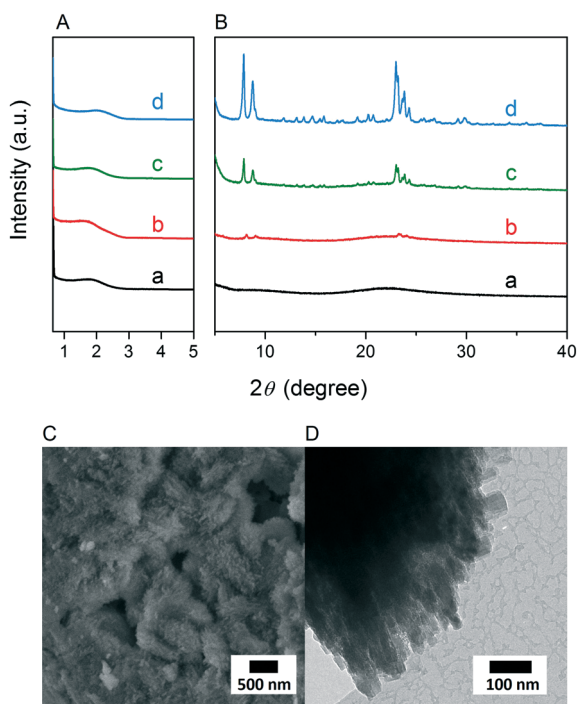


Fig. 12 (A) Small-angle and (B) wide-angle XRD patterns of the as-synthesized materials from a composition gel of  $\text{K}_2\text{O}:\text{SiO}_2:\text{Al}_2\text{O}_3:\text{CTABr}:\text{H}_2\text{O} = 12:95:5:4000$  after (a) 2, (b) 4, (c) 6 and (d) 8 days synthesis; (C) SEM and (D) TEM images of the as-synthesized material obtained after 8 days synthesis using the above recipe.

$\text{H}_2\text{O}/\text{Si} = 42.1$   
 $T = 413 \text{ K}$   
 Time: 8 days

Amorphous
Meso ZSM-5
ZSM-48

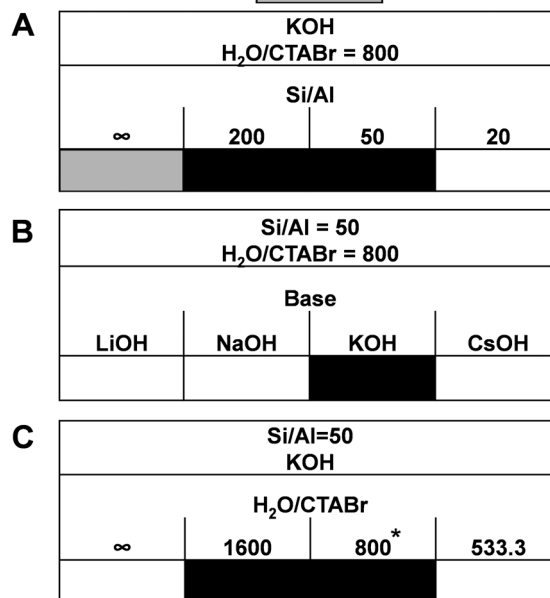


Fig. 13 Phase diagrams obtained using CTABr as SDA by varying parameters of (A) Al content, (B) type of base, and (C) CTA concentration. \*Success rate: 2 out of 5 synthesis.

establishing solid certainty on the validity of this result, we have reproduced the synthesis on 5 occasions, using different and sterile autoclaves for each experiment. It turns out that only 2 out of these 5 occasions succeeded, while the other 3 cases resulted in the formation of amorphous silica. Differently, in the case of using CTAOH as SDA, we always obtained the desired crystalline zeolite material.

As seen in Fig. 13, when CTABr is used as SDA, variation of the parameters results in similar materials as obtained

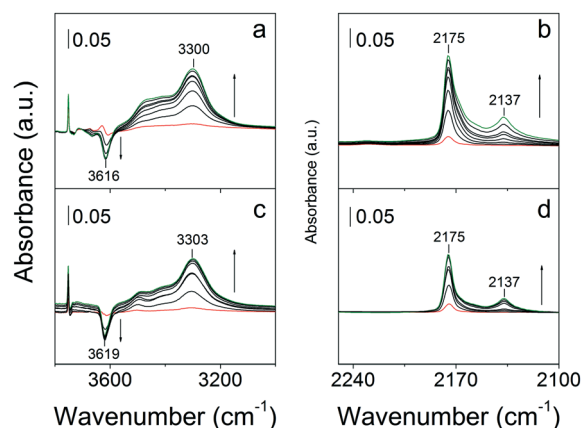
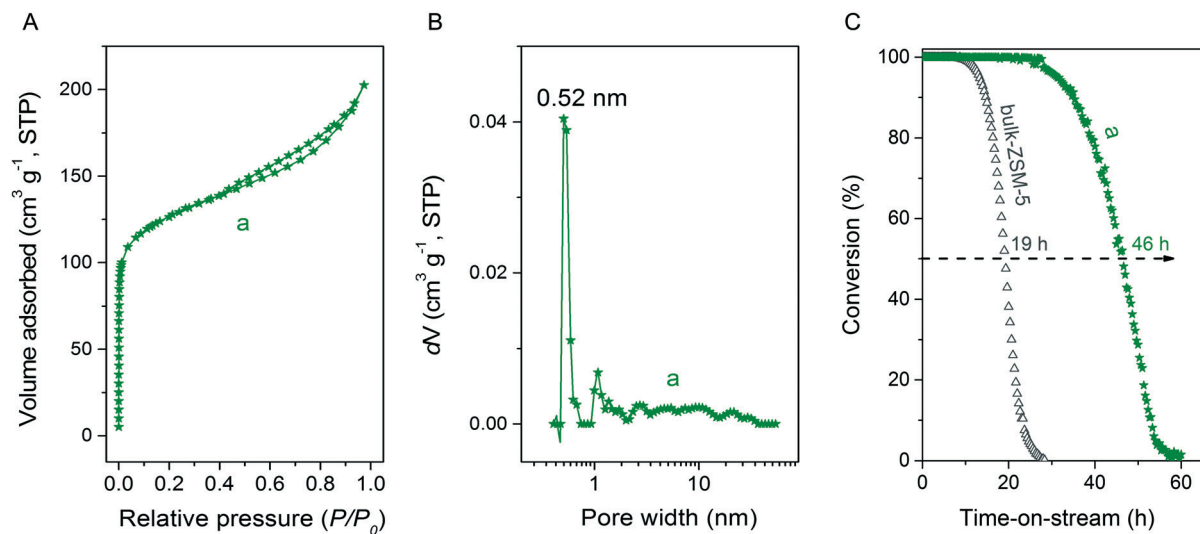


Fig. 14 (Left) Hydroxyl and (right) CO stretch regions in the FTIR spectra of bulk-ZSM-5 (a and b) and MFI(5CTABr, K, 0.96Al) (c and d, H form) recorded at 77 K. The spectra were normalized by the weight of the catalysts.





**Fig. 15** (A) Ar physisorption isotherm, (B) the corresponding pore size distribution and (C) methanol conversion as a function of time on stream in the MTH reaction for MFI(5CTABr, K, 0.96Al) (H form). Catalytic performance of bulk-ZSM-5 in MTH reaction was also shown in (C) for comparison.

with CTAOH. Without Al in the synthesis gel, ZSM-48 zeolite was obtained, controlling the Si/Al ratio in the 50–200 range results in ZSM-5 zeolite formation, and high Al content in the gel (Si/Al = 20) results in amorphous silica. Amorphous silica was obtained when applying LiOH, NaOH and CsOH as the base instead of KOH. Using CTABr at a molar ratio  $H_2O/CTABr = 800\text{--}1600$  leads to ZSM-5 zeolite formation, while without CTABr or with higher CTABr concentration ( $H_2O/CTABr = 533.3$ ) only amorphous silica was formed.

Fig. 14 shows the hydroxyl and CO stretch regions in the FTIR spectra of bulk-ZSM-5 and MFI(5CTABr, K, 0.96Al) recorded at 77 K. The two zeolites show an OH stretching band around  $3300\text{ cm}^{-1}$ , characteristic for strongly acidic bridging hydroxyl groups that are perturbed by CO.<sup>59,60</sup> They involve, for both cases, a red shift of  $\sim 316\text{ cm}^{-1}$  with respect to unperturbed bridging OH groups.<sup>10</sup> The equal red shift for these two materials implies that the Brønsted acid sites are similar in strength. In the carbonyl stretching region, two bands at  $2175\text{ cm}^{-1}$  and  $2137\text{ cm}^{-1}$  can be observed, which belong to CO adsorption on Brønsted acidic sites and physisorbed CO, respectively.<sup>10</sup> The frequency of CO coordinating to the Brønsted acid sites does not depend on the morphology of these two ZSM-5 zeolite.

Ar physisorption isotherm and PSD for MFI(5CTABr, K, 0.96Al) zeolite are shown in Fig. 15. The additional presence of mesoporosity in the zeolite is evident from the H4 type hysteresis loop in the Ar physisorption isotherm. The strong uptake at low relative pressure confirms the presence of micropores. The PSD indicates the presence of mesopores, next to the micropore system of ZSM-5. Table 2 further shows that this hierarchical zeolite has very favorable textural properties and, most notably, a high mesopore volume ( $0.11\text{ cm}^3\text{ g}^{-1}$ ). The potential of this mesoporous ZSM-5 zeolite in acid catalysis was evaluated by determining its catalytic performance in the MTH reaction. Fig. 15C shows methanol con-

version as function of time on stream for MFI(5CTABr, K, 0.96Al) and bulk-ZSM-5. The hierarchical ZSM-5 zeolite showed much longer lifetime (46 h) than bulk-ZSM-5 (19 h). As the elemental analysis and <sup>27</sup>Al NMR data confirm that these samples contain a similar amount of framework Al (Table 2), the greatly improved performance can be attributed to the smaller crystal domains in the hierarchical zeolite, effectively reducing mass transport limitations. The product distribution for MFI(5CTABr, K, 0.96Al) is similar with the one observed for bulk-ZSM-5 after 1 h time on stream, in which the main products are ethylene, propylene and C<sub>4+</sub> hydrocarbons.

## 4. Conclusions

In this work, we explored the conditions under which hierarchical ZSM-5 zeolite can be obtained in a one-pot synthesis procedure using CTA as the only template. A key aspect in these syntheses is that a mesoporous silica–alumina precursor is obtained initially which can transform to mesoporous zeolite through dissolution of silicate species at temperatures conducive to zeolite nucleation in the presence of CTA *via* a dissolution–recrystallization mechanism. We varied the base (LiOH, NaOH, KOH, RbOH and CsOH), the  $H_2O/CTA$  ratio, the Al content and the counter ion of CTA ( $Br^-$  or  $OH^-$ ).

Mesoporous ZSM-5 zeolite can be obtained in this way in the KOH/CTAOH/SiO<sub>2</sub> system at  $H_2O/CTA$  ratios in the 800–3200 range. Without CTAOH, a mixture of amorphous silica and  $\alpha$ -quartz was obtained, while a too high  $H_2O/CTA$  did not allow fast enough dissolution of silicate species, consistent with the known role of quaternary ammonium cations in stabilizing silica. While KOH and RbOH allowed obtaining hierarchical ZSM-5 zeolite in this way, the use of NaOH and CsOH as base mainly led to amorphous silica. That is a too small or too large alkali cation impedes silica dissolution.



For LiOH, this was also the case with an additional lithium silicate being obtained in that particular case. The conclusion that solubilisation of silica is too slow with LiOH, NaOH and CsOH is corroborated by the finding that seeding the synthesis with ZSM-5 resulted in formation of mesoporous ZSM-5 zeolites in all cases. Our results also point out the necessity of Al in the synthesis gel for crystallizing ZSM-5 zeolite. Without Al, only ZSM-48 was obtained. Setting the Si/Al ratio in the 50–200 range in the gel resulted in hierarchical ZSM-5. Higher Al content in the gel (Si/Al = 20) did not allow obtaining zeolite, although again the use of seeds facilitated ZSM-5 crystallization in the form of nano-needles with uniform thickness. This result indicates an important role of Al concentration in zeolite nucleation. Finally, replacing CTAOH with CTABr led to similar results although the reproducibility of such syntheses was found to be lower. A highly crystalline, free from extraframework Al and hierarchical ZSM-5 synthesized from a gel with KOH as base, H<sub>2</sub>O/CTAOH = 800, Si/Al = 50 and CTAOH as the template displays the highest catalytic performance in the MTH reaction, clearly outperforming bulk ZSM-5. An important implication of this work is that care has to be taken when exploring the use of organic templates in the synthesis of hierarchical zeolites using NaOH as mineralizing base. Stabilizing an amorphous silica precursor by Na<sup>+</sup> at temperatures at which zeolite nucleation can in principle proceed may obscure the potential of organic surfactants to direct silicate structures at the micro- and mesoscale.

## Conflicts of interest

There are no conflicts to declare.

## Acknowledgements

L. M. acknowledges financial support from the China Scholarship Council, A. M. Elemans-Mehring for ICP-OES analysis, and the Soft Matter Cryo-TEM Research Unit of Eindhoven University of Technology for access to TEM facilities. E. J. M. H. and M. G. G. thank The Netherlands Organization for Scientific Research (TOP grant).

## References

- 1 K. Na, M. Choi and R. Ryoo, *Microporous Mesoporous Mater.*, 2013, **166**, 3–19.
- 2 M. E. Davis, *Nature*, 2002, **417**, 813–821.
- 3 V. Valtchev and L. Tosheva, *Chem. Rev.*, 2013, **113**, 6734–6760.
- 4 D. Verboekend and J. Pérez-Ramírez, *Catal. Sci. Technol.*, 2011, **1**, 879–890.
- 5 K. Li, J. Valla and J. Garcia-Martinez, *ChemCatChem*, 2014, **6**, 46–66.
- 6 S. Mitchell, A. B. Pinar, J. Kenvin, P. Crivelli, J. Kärger and J. Pérez-Ramírez, *Nat. Commun.*, 2015, **6**, 8633–8645.
- 7 M. Hartmann, A. G. Machoke and W. Schwieger, *Chem. Soc. Rev.*, 2016, **45**, 3313–3330.
- 8 K. Moller and T. Bein, *Chem. Soc. Rev.*, 2013, **42**, 3689–3707.
- 9 L. Meng, X. Zhu and E. J. M. Hensen, *ACS Catal.*, 2017, **7**, 2709–2719.
- 10 L. Meng, X. Zhu, B. Mezari, R. Pestman, W. Wannapakdee and E. J. M. Hensen, *ChemCatChem*, 2017, DOI: 10.1002/cctc.201700916.
- 11 D. H. Olson, G. T. Kokotailo, S. L. Lawton and W. M. Meier, *J. Phys. Chem.*, 1981, **85**, 2238–2243.
- 12 J. Pérez-Ramírez, C. H. Christensen, K. Egeblad, C. H. Christensen and J. C. Groen, *Chem. Soc. Rev.*, 2008, **37**, 2530–2542.
- 13 W. J. Roth, P. Nachtigall, R. E. Morris and J. Čejka, *Chem. Rev.*, 2014, **114**, 4807–4837.
- 14 H. Zhang, L. Wang, D. Zhang, X. Meng and F.-S. Xiao, *Microporous Mesoporous Mater.*, 2016, **233**, 133–139.
- 15 W. Han, Y. Jia, G. Xiong and W. Yang, *Sci. Technol. Adv. Mater.*, 2007, **8**, 101–105.
- 16 B. Li, Z. Hu, B. Kong, J. Wang, W. Li, Z. Sun, X. Qian, Y. Yang, W. Shen, H. Xu and D. Zhao, *Chem. Sci.*, 2014, **5**, 1565–1573.
- 17 M. Choi, K. Na, J. Kim, Y. Sakamoto, O. Terasaki and R. Ryoo, *Nature*, 2009, **461**, 246–249.
- 18 X. Zhang, D. Liu, D. Xu, S. Asahina, K. A. Cychoz, K. V. Agrawal, Y. Al Wahedi, A. Bhan, S. Al Hashimi, O. Terasaki, M. Thommes and M. Tsapatsis, *Science*, 2012, **336**, 1684–1687.
- 19 W. Park, D. Yu, K. Na, K. E. Jelfs, B. Slater, Y. Sakamoto and R. Ryoo, *Chem. Mater.*, 2011, **23**, 5131–5137.
- 20 F.-S. Xiao, L. Wang, C. Yin, K. Lin, Y. Di, J. Li, R. Xu, D. S. Su, R. Schlögl, T. Yokoi and T. Tatsumi, *Angew. Chem.*, 2006, **118**, 3162–3165.
- 21 K. Egeblad, C. H. Christensen, M. Kustova and C. H. Christensen, *Chem. Mater.*, 2008, **20**, 946–960.
- 22 H. Wang and T. J. Pinnavaia, *Angew. Chem., Int. Ed.*, 2006, **45**, 7603–7606.
- 23 B. M. Lok, T. R. Cannan and C. A. Messina, *Zeolites*, 1983, **3**, 282–291.
- 24 C. T. Kresge, M. E. Leonowicz, W. J. Roth, J. C. Vartuli and J. S. Beck, *Nature*, 1992, **359**, 710–712.
- 25 A. Karlsson, M. Stöcker and R. Schmidt, *Microporous Mesoporous Mater.*, 1999, **27**, 181–192.
- 26 L. Huang, W. Guo, P. Deng, Z. Xue and Q. Li, *J. Phys. Chem. B*, 2000, **104**, 2817–2823.
- 27 Q. Cai, W.-Y. Lin, F.-S. Xiao, W.-Q. Pang, X.-H. Chen and B.-S. Zou, *Microporous Mesoporous Mater.*, 1999, **32**, 1–15.
- 28 Z. Luan, C.-F. Cheng, W. Zhou and J. Klinowski, *J. Phys. Chem.*, 1995, **99**, 1018–1024.
- 29 X. S. Zhao, G. Q. Lu and G. J. Millar, *Ind. Eng. Chem. Res.*, 1996, **35**, 2075–2090.
- 30 J. Y. Ying, C. P. Mehnert and M. S. Wong, *Angew. Chem., Int. Ed.*, 1999, **38**, 56–77.
- 31 M. Liu, J. Li, W. Jia, M. Qin, Y. Wang, K. Tong, H. Chen and Z. Zhu, *RSC Adv.*, 2015, **5**, 9237–9240.
- 32 Z. Wang, C. Li, H. J. Cho, S.-C. Kung, M. A. Snyder and W. Fan, *J. Mater. Chem.*, 2015, **3**, 1298–1305.
- 33 Y. Zhu, Z. L. Hua, J. Zhou, L. J. Wang, J. J. Zhao, Y. Gong, W. Wu, M. L. Ruan and J. L. Shi, *Chem. – Eur. J.*, 2011, **17**, 14618–14627.



- 34 X. Zhou, H. Chen, Y. Zhu, Y. Song, Y. Chen, Y. Wang, Y. Gong, G. Zhang, Z. Shu, X. Cui, J. Zhao and J. Shi, *Chem. – Eur. J.*, 2013, **19**, 10017–10023.
- 35 P. Peng, Y. Wang, M. J. Rood, Z. Zhang, F. Subhan, Z. Yan, L. Qin, Z. Zhang, Z. Zhang and X. Gao, *CrystEngComm*, 2015, **17**, 3820–3828.
- 36 T. Prasomsri, W. Jiao, S. Z. Weng and J. Garcia Martinez, *Chem. Commun.*, 2015, **51**, 8900–8911.
- 37 X. Zhu, M. G. Goesten, A. J. J. Koekkoek, B. Mezari, N. Kosinov, G. Filonenko, H. Friedrich, R. Rohling, B. M. Szyja, J. Gascon, F. Kapteijn and E. J. M. Hensen, *Chem. Sci.*, 2016, **7**, 6506–6513.
- 38 L. Meng, B. Mezari, M. G. Goesten and E. J. M. Hensen, *Chem. Mater.*, 2017, **29**, 4091–4096.
- 39 D. Xu, Z. Jing, F. Cao, H. Sun and S. Che, *Chem. Mater.*, 2014, **26**, 4612–4619.
- 40 M. Thommes, *Chem. Ing. Tech.*, 2010, **82**, 1059–1073.
- 41 K. S. W. Sing and R. T. Williams, *Adsorpt. Sci. Technol.*, 2004, **22**, 773–782.
- 42 U. Olsbye, S. Svelle, M. Bjørgen, P. Beato, T. V. W. Janssens, F. Joensen, S. Bordiga and K. P. Lillerud, *Angew. Chem., Int. Ed.*, 2012, **51**, 5810–5831.
- 43 D. Mores, J. Kornatowski, U. Olsbye and B. M. Weckhuysen, *Chem. – Eur. J.*, 2011, **17**, 2874–2884.
- 44 X. Huang, H. Li, W. D. Xiao and D. Chen, *Chem. Eng. J.*, 2016, **299**, 263–275.
- 45 K. Hemelsoet, J. Van der Mynsbrugge, K. De Wispelaere, M. Waroquier and V. Van Speybroeck, *ChemPhysChem*, 2013, **14**, 1526–1545.
- 46 M. Bjørgen, S. Svelle, F. Joensen, J. Nerlov, S. Kolboe, F. Bonino, L. Palumbo, S. Bordiga and U. Olsbye, *J. Catal.*, 2007, **249**, 195–207.
- 47 S. Svelle, F. Joensen, J. Nerlov, U. Olsbye, K. P. Lillerud, S. Kolboe and M. Bjørgen, *J. Am. Chem. Soc.*, 2006, **128**, 14770–14771.
- 48 Y. V. Kissin, *Catal. Rev.: Sci. Eng.*, 2001, **43**, 85–146.
- 49 Z. Liu, X. Dong, Y. Zhu, A.-H. Emwas, D. Zhang, Q. Tian and Y. Han, *ACS Catal.*, 2015, **5**, 5837–5845.
- 50 X. Zhu, L. Wu, P. C. M. M. Magusin, B. Mezari and E. J. M. Hensen, *J. Catal.*, 2015, **327**, 10–21.
- 51 J. R. Jacquin and M. Tomozawa, *J. Non-Cryst. Solids*, 1995, **190**, 233–237.
- 52 C. S. Cundy and P. A. Cox, *Chem. Rev.*, 2003, **103**, 663–702.
- 53 P. W. J. G. Wijnens, T. P. M. Beelen, J. W. de Haan, C. P. J. Rummens, L. J. M. van de Ven and R. A. van Santen, *J. Non-Cryst. Solids*, 1989, **109**, 85–94.
- 54 P. W. J. G. Wijnens, T. P. M. Beelen, J. W. De Haan, L. J. M. Van De Ven and R. A. Van Santen, *Colloids Surf.*, 1990, **45**, 255–268.
- 55 G. Majano, A. Darwiche, S. Mintova and V. Valtchev, *Ind. Eng. Chem. Res.*, 2009, **48**, 7084–7091.
- 56 R. F. Lobo and H. van Koningsveld, *J. Am. Chem. Soc.*, 2002, **124**, 13222–13230.
- 57 C. E. A. Kirschhock, D. Liang, G. V. Tendeloo, A. Fécant, G. Hastoye, G. Vanbutsele, N. Bats, E. Guillon and J. A. Martens, *Chem. Mater.*, 2009, **21**, 371–380.
- 58 L. Wu, P. C. M. M. Magusin, V. Degirmenci, M. Li, S. M. T. Almutairi, X. Zhu, B. Mezari and E. J. M. Hensen, *Microporous Mesoporous Mater.*, 2014, **189**, 144–157.
- 59 S. M. T. Almutairi, B. Mezari, E. A. Pidko, P. C. M. M. Magusin and E. J. M. Hensen, *J. Catal.*, 2013, **307**, 194–203.
- 60 M. S. Holm, S. Svelle, F. Joensen, P. Beato, C. H. Christensen, S. Bordiga and M. Bjørgen, *Appl. Catal., A*, 2009, **356**, 23–30.

